Eur. Phys. J. A (2018) **54**: 56
DOI 10.1140/epja/i2018-12491-8

THE EUROPEAN PHYSICAL JOURNAL A

Regular Article – Experimental Physics

# Role of partial linear momentum transfer on incomplete fusion reaction

Sabir Ali[1,a], Tauseef Ahmad[2], Kamal Kumar[2], Muntazir Gull[2,b], I.A. Rizvi[2], Avinash Agarwal[3], S.S. Ghugre[4], A.K. Sinha[4], and A.K. Chaubey[5]

[1] MANUU Polytechnic Darbhanga, Maulana Azad National Urdu University, Hyderabad 500032, India
[2] Department of Physics, Aligarh Muslim University, Aligarh 202002, India
[3] Department of Physics, Bareilly College, Bareilly 243005, India
[4] UGC-DAE Consortium for Scientific Research, Kolkata 700098, India
[5] Department of Physics, Addis Ababa University, P.O. Box 1176, Addis Ababa, Ethiopia

Received: 9 September 2017 / Revised: 25 January 2018
Published online: 16 April 2018 – 
Communicated by R.K. Bhandari

**Abstract.** Measurements of forward recoil range distributions (FRRDs) of the evaporation residues, populated in the $^{20}$Ne + $^{51}$V reaction at $E_{lab} \approx 145$ MeV, have been carried out using the offline characteristic $\gamma$-ray detection method. The observation does corroborate the presence of complete fusion (CF) process in the population of p$xn$ channel residues and both complete as well as incomplete fusion (ICF) processes in the population of $\alpha$ emitting channel residues. The FRRDs of p$xn$ channel residues comprise single peak only, whereas $\alpha$ emitting channel residues have multiple peaks in their FRRDs. CF cross section data were used to extract the fusion functions. Extracted fusion functions were found to be suppressed with respect to the universal fusion function which is used as a uniform standard reference. The observed contribution arising from the ICF process in the population of $\alpha$ emitting channel residues is explained in terms of breakup fusion model.

## 1 Introduction

Study of fusion reaction using the loosely as well as tightly bound projectile has been a subject of great concern over the last few decades [1–4]. Several studies have been carried out so far to observe the influence of various entrance channel parameters on incomplete fusion reaction [5,6]. Incident projectiles with beam energy above the Coulomb barrier interact with the target nuclei and lead to different nuclear reactions. One of the possible reaction channel is the direct complete fusion (DCF) process in which the entire projectile fuses with the target nucleus, surviving the breakup process, leading to a complete transfer of incident momentum to the resulting compound system. On the other hand, breakup of the incident projectile in the periphery of the target's nuclear field opens up a doorway to a number of new reaction channels. When all the breakup fragments of the incident projectile fuse with the target nucleus one after the other, the process is called sequential complete fusion (SCF). It is also possible that only a part of the incident projectile fuses with the target nucleus leading to a partial transfer of incident momentum to the resulting compound system through the incomplete fusion (ICF) process. There is also the possibility that none of the breakup fragments are able to get fused with the target nucleus leading to non capture breakup (NCBU) process. SCF and DCF lead to the formation of the same compound nucleus with the same excitation energy and transferred momentum, hence, experimentally it is not possible to differentiate between these two processes. Thus only complete fusion (CF) cross section which is the algebraic sum of SCF and DCF, *i.e.* $\sigma_{CF} = \sigma_{SCF} + \sigma_{DCF}$, can be measured experimentally.

One of the most widely used methods for the confirmation of evaporation residues (ERs) populated through different fusion processes is to either directly observe the residues [7] or indirectly identify the residues through their characteristic $\gamma$-rays [8]. Another method which is utilized in the present work for differentiating between the ERs populated through CF and/or ICF processes is the measurement of forward recoil range distribution (FRRD) of the populated ERs.

Among all the possible reaction channels in heavy ion induced reactions at $E_{lab} \approx 7$ MeV/nucleon, CF and ICF processes were found to be the most dominant [9]. CF and ICF processes can be differentiated on account of quantum of linear momentum transferred (LMT) from incident projectile to the resulting compound system [10]. Since

[a] e-mail: sabir@manuu.ac.in
[b] e-mail: muntazirgull1@gmail.com

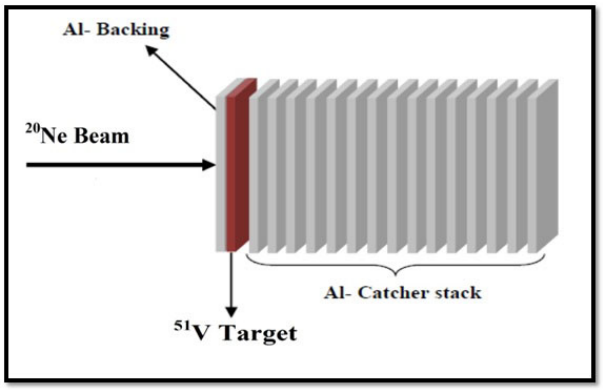


**Fig. 1.** (Color online) A schematic diagram of target-catcher foil arrangement used for the study of forward recoil range distributions of ERs populated in the $^{20}\mathrm{Ne} + {}^{51}\mathrm{V}$ reaction at $E_{lab} \approx 145\,\mathrm{MeV}$.

the observation of forward emitted fast particles by Britt and Quinton [11], the phenomenon of projectile breakup has been investigated by many authors for loosely as well as tightly bound systems [12,13]. However, a consistent appreciation of the projectile breakup process, now referred to as ICF, only emerged with the work of Inamura *et al.* [14]. The breakup probability of the incident projectile was found to influence the contribution arising from the ICF cross section towards the total fusion (TF) cross section. It has been reported by several authors [15–17] that higher the breakup probability of the incident projectile, higher is the contribution of ICF cross section to the TF cross section.

So far, several methodologies have been proposed to estimate the magnitude of ICF contributions to the TF cross section. One of the most general methods utilized for this purpose is to compare the prediction of coupled channels (CC) or one dimension barrier penetration model (1D-BPM) calculation, which inherently assumes that the probability of the compound nucleus formation $P_{CN} = 1$, with the experimental fusion cross section data. It has been observed that above the barrier energy CF cross section is suppressed as compared to the prediction of CC or 1D-BPM calculations [18,19]. The extent of fusion suppression was found to be influenced by various entrance channel parameters *viz.* Coulomb repulsion, breakup threshold energy ($E_{B.U}$) of the incident projectile, mass asymmetry, deformation parameters, etc. Another such method to observe the influence of entrance channel parameters on ICF reaction is to compare the fusion cross section data with the Universal fusion function (UFF), prescribed by Canto *et al.* [20], which is based on Wong's approximation [21] for the fusion cross section.

A majority of CF suppression work carried out earlier was concerned mainly with the loosely bound projectile with $E_{B.U}$ in the range of $\approx$ 1.5 to 3 MeV [22,23]. On the other hand several works have been reported dealing with fusion incompleteness involving tightly bound projectiles like $^{12,13}$C, $^{16,18}$O, etc. having $E_{B.U}$ in the range of $\approx$ 7 to 11 MeV [24–26]. In spite of the enormous work already carried out, there is severe scarcity of data on ICF reaction involving projectile with $E_{B.U}$ in the range of 3 to 6 MeV. Thus, in order to bridge the gap between the study of loosely and tightly bound projectile's ICF reaction, the present work is carried out using $^{20}$Ne as projectile having $E_{B.U}$ of 4.7 MeV. The main objective of the present work is to study the role of projectile $E_{B.U}$ on ICF reaction by measuring the FRRDs of the ERs populated in the $^{20}\mathrm{Ne} + {}^{51}\mathrm{V}$ reaction at $E_{lab} \approx 145\,\mathrm{MeV}$. This work can be considered as a complement to our previous work in which we have studied the excitation function (EF) of ERs populated in $^{20}\mathrm{Ne} + {}^{51}\mathrm{V}$ reaction at energies $E_{lab} \approx 82$–$145\,\mathrm{MeV}$ [27]. The present work is organized as follows. A brief experimental detail related to the present work is given in sect. 2, whereas the analysis and interpretation of the results are given in sect. 3. Finally, the conclusion drawn from the current study is given in sect. 4.

## 2 Experimental details

### 2.1 Target preparation and irradiation

Beams of $^{20}\mathrm{Ne}^{6+}$ at $E_{lab} \approx 145\,\mathrm{MeV}$ from Variable Energy Cyclotron Centre (VECC), Kolkata, India were used for the study of FRRDs using the target, which was a foil of $^{51}$V (99.97% pure), mounted normal to the beam axis. The target was placed in the form of a stack consisting of a $^{51}$V target foil followed by a series of thin Al-catcher foils for trapping the recoiling residues. For irradiation, the $^{51}$V target of thickness $\approx 250\,\mu\mathrm{g/cm^2}$, evaporated onto an Al support of thickness $\approx 200\,\mu\mathrm{g/cm^2}$, was used. This combination of Al support and $^{51}$V target was mounted such that the Al support faced the incident ion beam, followed by a stack of 20 thin Al-catcher foils. The thickness of Al-catcher foil ranges from 100 to $150\,\mu\mathrm{g/cm^2}$. The thicknesses of Al-catcher and target foils had been determined prior to use by weighing as well as by the $\alpha$ energy loss method. The thicknesses of Al-catcher foils were taken in such a manner that the recoil range of the heaviest ER, populated in the $^{20}\mathrm{Ne} + {}^{51}\mathrm{V}$ reaction at $E_{lab} \approx 145\,\mathrm{MeV}$, falls within the cumulative thickness of the Al-catcher foils. The $^{20}\mathrm{Ne}^{6+}$ beam was collimated to a spot of diameter 8 mm and the stack was irradiated with beam current varying between 15 to 20 nA for $\approx$ 11 hrs. Beam flux was calculated by measuring the total charge collected in the Faraday cup, placed behind the target-catcher assembly. A schematic diagram of the target-catcher foil arrangement is shown in fig. 1.

### 2.2 Post irradiation analysis and identification of the residues

Following the irradiation, $\gamma$-ray activities induced in each Al-catcher foil were recorded using a 60 cc HPGe detector coupled to a PC based data acquisition system developed by VECC. Activities induced in each Al-catcher foil were recorded several times immediately after the irradiation was over and continued for few days at an interval varying from 15 minutes to several hours. The resolution of the HPGe detector was found to be 1.9 keV

**Table 1.** List of observed reaction channels populated in the $^{20}$Ne+$^{51}$V reaction at $E_{lab} \approx 145$ MeV are given in the first column along with the half-lives in the second column and other columns have spectroscopic properties taken from ref. [29].

| Reaction | Half-life | $J^{\pi}$ | $E_{\gamma}$ (keV) | $I^{\gamma}$ |
|---|---|---|---|---|
| $^{51}$V($^{20}$Ne, p3$n$)$^{67}$Ge | 18.9 min | $1/2^-$ | 167.0 | 84.4 |
| | | | 1472.5 | 4.9 |
| $^{51}$V($^{20}$Ne, p4$n$)$^{66}$Ge | 2.26 hrs | $0^+$ | 381.8 | 28.0 |
| | | | 272.9 | 10.4 |
| $^{51}$V($^{20}$Ne, $\alpha$2$n$)$^{65}$Ga | 15.2 min | $3/2^-$ | 115.0 | 54 |
| | | | 153.0 | 8.9 |
| $^{51}$V($^{20}$Ne, $\alpha$p3$n$)$^{63}$Zn | 38.5 min | $3/2^-$ | 669.6 | 8.0 |
| | | | 962.0 | 6.5 |
| $^{51}$V($^{20}$Ne, $\alpha$p4$n$)$^{62}$Zn | 9.18 hrs | $0^+$ | 596.5 | 26.0 |
| $^{51}$V($^{20}$Ne, 2$\alpha$2$n$)$^{61}$Cu | 3.33 hrs | $3/2^-$ | 282.9 | 12.2 |
| | | | 656.0 | 10.7 |
| $^{51}$V($^{20}$Ne, 2$\alpha$3$n$)$^{60}$Cu | 23.7 min | $2^+$ | 1332.5 | 88.0 |
| | | | 826.0 | 21.7 |
| $^{51}$V($^{20}$Ne, 2$\alpha$2p)$^{61}$Co | 1.65 hrs | $7/2^-$ | 908.6 | 3.6 |

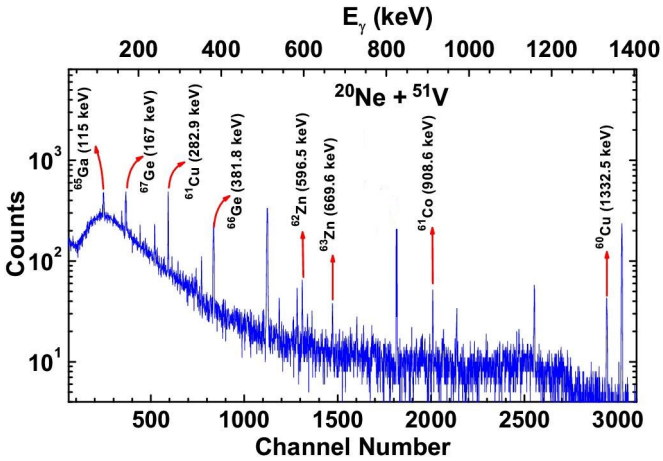


**Fig. 2.** (Color online) Recorded $\gamma$-ray energy spectrum of the residues populated in the $^{20}$Ne + $^{51}$V reaction at $E_{lab} \approx$ 145 MeV.

for 1.33 MeV $\gamma$-ray from the $^{60}$Co source. The geometry dependent photopeak detection efficiency of the HPGe detector at various source-detector separations was measured using the $^{152}$Eu source of known strength. The $\gamma$-ray spectroscopy software package RADWARE [28] has been used for analyzing the spectrum. The activities of the observed radionuclides populated in the $^{20}$Ne + $^{51}$V reaction at $E_{lab} \approx 145$ MeV, listed in table 1, were extracted from the recorded $\gamma$-ray spectra. A typical recorded $\gamma$-ray energy spectrum of the residues populated in the $^{20}$Ne + $^{51}$V reaction at $E_{lab} \approx 145$ MeV is shown in fig. 2. Various peaks observed in the $\gamma$-ray spectra were assigned to different residues on the basis of their characteristic $\gamma$-rays as well as their measured half-lives. The measured half-lives of the observed ERs were found to be in good agreement with their standard literature values. The nuclear spectroscopic data used in the evaluation and measurement of the cross sections were taken from the Radioactive Isotopes Data Table of Brown and Firestone [29].

The reaction cross sections of the observed ERs populated through different possible reaction channels were estimated using the standard formulation [8] given by

$$\sigma_r = \frac{A\lambda \exp(\lambda t_2)}{N_0 \theta \phi \epsilon_G K[1 - \exp(-\lambda t_1)][1 - \exp(-\lambda t_3)]}, \quad (1)$$

where the symbols have their usual meaning. Further detailed discussion about the reaction cross section formulation is given in ref. [27].

Various factors are likely to introduce error and uncertainty in the measured reaction cross sections of the populated ERs. Some of the potential sources of error in the present work are as follows: i) Non-uniformity in the thickness of the target foil leads to an uncertainty in determining the number of nuclei present in it. In order to check the uniformity of the target foil, the thickness of target foil was measured at a different position by the $\alpha$ energy loss method. The error arising due to the uncertainty in thickness of the target foil was found to be less than 3%. ii) Fluctuation in beam current leads to the variation in the flux of the incident projectile beam. Proper care was taken to keep the beam current constant. However, the error arising due to the fluctuation in beam current was found to be less than 3%. iii) Errors arising due to the geometry dependent detector efficiency, caused by the statistical uncertainty in the counts under the peak, were estimated to be less than 5%. iv) The error contributed due to the dead time of the spectrometer was kept below 10% by suitably adjusting the sample-detector separation. v) Errors associated with the energy straggling of the ion-beam were estimated to be less than 2%. Efforts were made to minimize the uncertainty arising from all the sources and the overall error estimated in the present work does not exceed 20%.

## 3 Analysis and interpretation of results

In the $^{20}$Ne + $^{51}$V reaction at $E_{lab} \approx 145$ MeV a total of eight ERs, namely $^{67}$Ge (p3$n$), $^{66}$Ge (p4$n$), $^{65}$Ga ($\alpha$2$n$), $^{63}$Zn ($\alpha$p3$n$), $^{62}$Zn ($\alpha$p4$n$), $^{61}$Cu (2$\alpha$2$n$), $^{60}$Cu (2$\alpha$3$n$) and $^{61}$Co (2$\alpha$2p) were observed. Among the observed ERs, the $\alpha$ emitting channel residues ($^{65}$Ga, $^{63}$Zn, $^{62}$Zn, $^{61}$Cu, $^{60}$Cu, $^{61}$Co) are likely to get populated through the CF as well as ICF processes whereas the non-alpha channel residues ($^{67}$Ge, $^{66}$Ge) have the possibility of getting populated through the CF process only. Both CF and ICF are treated as two stage processes in which the first stage, known as "*fusion stage*", involves the amalgamation of all or part of the incident projectile with the target nucleus to form an excited intermediate compound system, and the second stage, called "*evaporation stage*", involves the de-excitation of the intermediate compound system via particle and $\gamma$-ray emission. The nature of the emitted particle

is governed by the excitation energy of the intermediate compound system. The intermediate compound systems formed through the CF and ICF processes differ from each other in terms of excitation energy and recoil range in the stopping medium. Intermediate compound system formed through the CF process recoils along the beam-axis with a recoil velocity and excitation energy governed totally by the incident energy of the projectile, whereas the intermediate compound system formed through a particular ICF process is endowed with an extended range of recoil velocity, recoil angle and excitation energy [30].

### 3.1 Forward recoil range distributions

FRRD of a given ER is the plot of normalized yield, obtained by dividing the fusion cross section of the reaction product (in mb) by the thickness of the catcher foil (in mg/cm$^2$), against the cumulative thickness of the Al-catcher foil (in $\mu$g/cm$^2$). FRRD represents the velocity distribution of the ER populated either through the CF and/or ICF processes in the stopping medium. The velocity distribution of the ERs will be symmetric about the recoiling velocity ($v_0$) of the intermediate compound system with a width which is governed by the mass or number of the emitted particles [30].

For a compound nucleus formed through the CF process, conservation of linear momentum leads to

$$v_0 = V_{CN} = \frac{\sqrt{2m_pE}}{M_{com}}, \qquad (2)$$

where $V_{CN}$ is the velocity of the compound nucleus, $m_p$ and $M_{com}$ are the masses of incident projectile and compound system, respectively, and $E$ is the incident energy of projectile in the laboratory frame. For an intermediate compound system formed through the ICF process, the recoil velocity of the intermediate compound system will be less than $v_0$. The linear momentum with which the ICF residues were populated must always be less than the incident linear momentum $p_{inc}$ because a fraction of the $p_{inc}$ is carried away by the spectator. If the projectile were a point object, $p_{inc}$ would be shared between the fusing fragment and the spectator in the ratio of their masses. Since the diameter of the projectile extends over a range of impact parameters and in general the spectator presumably breaks off from the outer surface of the projectile, linear momentum imparted to the intermediate compound system by a fusing fragment of mass $M_f$ emerging from the incident projectile of mass $M_p$ having linear momentum $p_{inc}$ will be equal to $(M_f/M_p)p_{inc}$.

#### 3.1.1 FRRD of evaporation residues populated through p$xn$ channels

Complete fusion of $^{20}$Ne projectile with the $^{51}$V target leads to the formation of an excited intermediate compound system $^{71}$As$^*$. The excited compound system further decays via the emission of particles and $\gamma$-rays leading to the formation of $^{67,66}$Ge isotopes through the p$xn$ ($x = 3, 4$) channel. As a representative case, the systematic for the formation of ER $^{67}$Ge through the p3$n$ channel may be given as

$$^{20}\mathrm{Ne} + {}^{51}\mathrm{V} \Rightarrow {}^{71}\mathrm{As}^*,$$
$$^{71}\mathrm{As}^* \Rightarrow {}^{67}\mathrm{Ge} + \mathrm{p}3n,$$

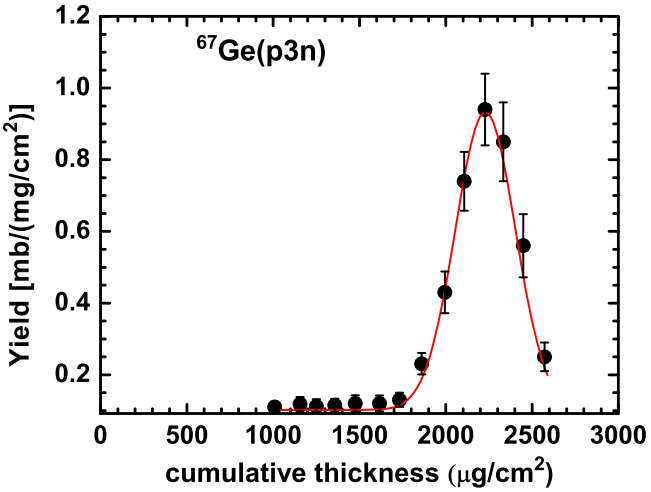


**Fig. 3.** (Color online) Experimentally measured FRRD of ER $^{67}$Ge populated through p3$n$ channel. Solid line through the data points are the Gaussian fit of the experimental data points (solid circles).

Figure 3 shows the FRRD of the ER $^{67}$Ge populated through the p3$n$ channel. As can be seen from fig. 3, the FRRD of the $^{67}$Ge residues consists of a single peak at 2229.6 $\mu$g/cm$^2$, suggesting a total linear momentum transfer from projectile to target through the CF of $^{20}$Ne projectile with the $^{51}$V target. Similarly, the FRRD of the $^{66}$Ge residues also comprises a single peak arising from the complete transfer of linear momentum from projectile to target, indicating the production of residues through the CF process only. The measured FRRDs of the observed CF residues $^{67}$Ge and $^{66}$Ge were found to be slightly different from the theoretical value predicted for the intermediate compound nucleus $^{71}$As using the code SRIM [31].

#### 3.1.2 FRRD of evaporation residues populated through $\alpha$ emitting channels

In the present work, a total of six $\alpha$ emitting channel residues, namely, $^{65}$Ga, $^{63}$Zn, $^{62}$Zn, $^{61}$Cu, $^{60}$Cu and $^{60}$Co were found to get populated through the $\alpha 2n$, $\alpha$p3$n$, $\alpha$p4$n$, $2\alpha 2n$, $2\alpha 3n$, and $2\alpha$2p channels, respectively. ERs populated through $\alpha$ emitting channels have the possibility of getting populated through the CF as well as ICF processes. The observed FRRDs of the ERs populated through the $\alpha$ emitting channels were resolved into multiple peaks. Particularly interesting is the FRRD of the ER $^{61}$Cu populated through the $2\alpha 2n$ channel, reflecting the interplay between the CF, ICF$^{\alpha}$ and ICF$^{2\alpha}$ processes through different decay modes. It can be inferred from fig. 4, showing the FRRD of ER $^{61}$Cu, that the FRRD

**Table 2.** Experimentally measured range integrated cross section $\sigma_{RRD}$ (mb) of the observed ERs populated in the $^{20}Ne + ^{51}V$ reaction at $E_{lab} \approx 145$ MeV along with the $Q$-value (MeV) and threshold energy $E_{thr}$ (MeV) for the CF, ICF$^{\alpha}$ and ICF$^{2\alpha}$ processes.

| Residues | $\sigma_{RRD}$ | $Q$-value (MeV) | | | $E_{thr}$ (MeV) | | |
|---|---|---|---|---|---|---|---|
| | (mb) | CF | ICF$^{\alpha}$ | ICF$^{2\alpha}$ | CF | ICF$^{\alpha}$ | ICF$^{2\alpha}$ |
| $^{67}$Ge (p3$n$) | $0.5 \pm 0.06$ | $-28.09$ | – | – | 39.10 | – | – |
| $^{66}$Ge (p4$n$) | $0.8 \pm 0.1$ | $-37.21$ | – | – | 51.81 | – | – |
| $^{65}$Ga ($\alpha$2$n$) | $22.3 \pm 2.9$ | $-15.15$ | $-10.42$ | – | 21.08 | 13.68 | – |
| $^{63}$Zn ($\alpha$p3$n$) | $56.7 \pm 5.6$ | $-30.96$ | $-26.23$ | – | 43.09 | 34.45 | – |
| $^{62}$Zn ($\alpha$p4$n$) | $45.4 \pm 6.4$ | $-40.07$ | $-35.34$ | – | 55.78 | 46.42 | – |
| $^{61}$Cu (2$\alpha$2$n$) | $114.9 \pm 14.3$ | $-18.34$ | $-13.52$ | $-6.36$ | 25.52 | 17.76 | 7.85 |
| $^{60}$Cu (2$\alpha$3$n$) | $30.5 \pm 4.5$ | $-30.05$ | $-25.23$ | $-18.07$ | 41.82 | 33.14 | 22.32 |
| $^{61}$Co (2$\alpha$2p) | $9.6 \pm 1.1$ | $-15.86$ | $-11.04$ | $-3.88$ | 22.07 | 14.50 | 4.79 |

comprises three peaks at different recoil ranges suggesting a multiple component of LMT from projectile to target through the CF, ICF$^{\alpha}$ and ICF$^{2\alpha}$ processes. The experimentally measured range integrated cross section of the observed ERs populated through CF, ICF$^{\alpha}$ and ICF$^{2\alpha}$ processes in the $^{20}Ne + ^{51}V$ reaction at $E_{lab} \approx 145$ MeV along with the $Q$-value and threshold energy ($E_{thr}$) are given in table 2.

1) ICF$^{2\alpha}$ *process:* the ICF$^{2\alpha}$ process involves the fusion of $^{12}$C, evolving from the breakup of the $^{20}$Ne projectile ($^{20}Ne \rightarrow {}^{12}C + {}^{8}Be(2\alpha)$), with the $^{51}$V target. The incident projectile $^{20}$Ne, having $\alpha$ cluster structure, comprises five $\alpha$ particles and the total linear momentum associated with the incident projectile is equally distributed among its five $\alpha$ constituents. In the case of the ICF$^{2\alpha}$ process only three $\alpha$ particles ($^{12}$C) fuse with the target nucleus leading to a transfer of (3/5) $p_{inc}$ from projectile to target, *i.e.* 60% of the incident linear momentum is transferred from projectile to target. Due to relatively lesser linear momentum transfer, the resulting reduced compound system will recoil to lesser distance in the recoiling medium. In fig. 4, the first peak at the lowest recoil range in FRRD of the $^{61}$Cu residue corresponds to the ICF$^{2\alpha}$ process.

$$^{20}Ne \Rightarrow {}^{12}C + {}^{8}Be(2\alpha),$$
$$E_{B.U} = 11.9\,\text{MeV}.$$

$^{12}$C, emerging from the breakup of $^{20}$Ne projectile, fuses with the $^{51}$V target leading to the formation of an incompletely fused compound system $^{63}$Cu$^{*}$ through the ICF$^{2\alpha}$ process. The excited incompletely fused compound system $^{63}$Cu$^{*}$ further decays via the 2$n$, 3$n$ and 2p channels to form the ERs $^{61}$Cu, $^{60}$Cu and $^{61}$Co, respectively. As an example the reaction mechanism for the formation of $^{61}$Cu residue through the ICF$^{2\alpha}$ process may be represented as

$$^{20}Ne(^{12}C + {}^{8}Be(2\alpha)) + {}^{51}V \Rightarrow {}^{63}Cu^{*} + {}^{8}Be(2\alpha)$$
$$^{63}Cu^{*} \Rightarrow {}^{61}Cu + 2n + {}^{8}Be(2\alpha),$$
$$(^{8}Be(2\alpha) \text{ as a spectator}).$$

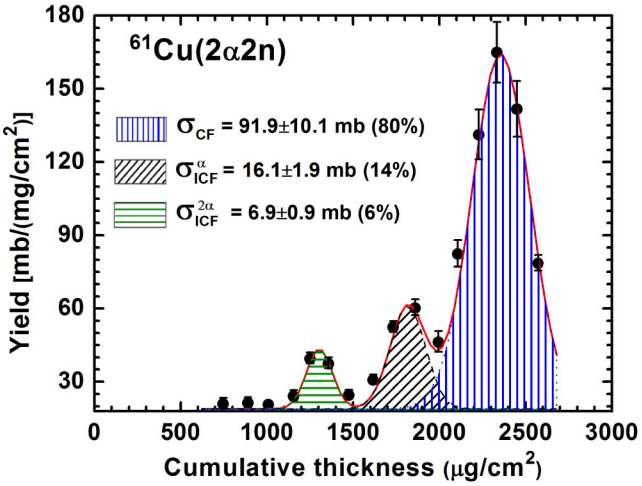


**Fig. 4.** (Color online) Experimentally measured FRRD of ER $^{61}$Cu populated through 2$\alpha$2$n$ channel. The relative contributions arising from CF, ICF$^{\alpha}$ and ICF$^{2\alpha}$ processes are also mentioned in the figure. Solid lines through the data points are the Gaussian fit of the experimental data points (solid circles).

2) ICF$^{\alpha}$ *process:* in the case of the ICF$^{\alpha}$ process only (4/5) $p_{inc}$ *i.e.* 80% of the incident linear momentum is transferred to the $^{51}$V target through the fusion of $^{16}$O, resulting from the breakup of $^{20}$Ne projectile ($^{20}Ne \rightarrow {}^{16}O + \alpha$). The second peak at slightly higher recoil range in FRRD of ER $^{61}$Cu (fig. 4) corresponds to the ICF$^{\alpha}$ process.

$$^{20}Ne \Rightarrow {}^{16}O + \alpha,$$
$$E_{B.U} = 4.7\,\text{MeV}.$$

The excited reduced compound system $^{67}$Ga$^{*}$, formed through the fusion of $^{16}$O with $^{51}$V target will further decay to $^{61}$Cu, $^{60}$Cu and $^{61}$Co residues through the $\alpha$2$n$, $\alpha$3$n$ and $\alpha$2p channels, respectively. As a representative case, the mechanism involved in the formation of $^{61}$Cu residue through the ICF$^{\alpha}$ process may be

**Table 3.** Experimental measured most probable range $R_{exp}$ as well as theoretically calculated range $R_{theo}$ using the code SRIM, in Al-catcher foils in unit of $\mu$g/cm$^2$, for the experimentally observed reaction channels in $^{20}$Ne+$^{51}$V reaction at $E_{lab} \approx 145$ MeV.

| Residues | CF | | ICF$^{\alpha}$ | | ICF$^{2\alpha}$ | |
|---|---|---|---|---|---|---|
| | $R_{exp}$ ($\mu$g/cm$^2$) | $R_{theo}$ ($\mu$g/cm$^2$) | $R_{exp}$ ($\mu$g/cm$^2$) | $R_{theo}$ ($\mu$g/cm$^2$) | $R_{exp}$ ($\mu$g/cm$^2$) | $R_{theo}$ ($\mu$g/cm$^2$) |
| $^{67}$Ge (p3$n$) | $2230 \pm 330$ | 2308 | – | – | – | – |
| $^{66}$Ge (p4$n$) | $2456 \pm 398$ | 2308 | – | – | – | – |
| $^{65}$Ga ($\alpha$2$n$) | $2201 \pm 299$ | 2308 | $1458 \pm 268$ | 1817 | – | – |
| $^{63}$Zn ($\alpha$p3$n$) | $2385 \pm 396$ | 2308 | $1767 \pm 270$ | 1817 | – | – |
| $^{62}$Zn ($\alpha$p4$n$) | $2396 \pm 415$ | 2308 | $1666 \pm 282$ | 1817 | – | – |
| $^{61}$Cu (2$\alpha$2$n$) | $2355 \pm 351$ | 2308 | $1817 \pm 231$ | 1817 | $1304 \pm 198$ | 1474 |
| $^{60}$Cu (2$\alpha$3$n$) | $2304 \pm 327$ | 2308 | $1853 \pm 217$ | 1817 | $1424 \pm 162$ | 1474 |
| $^{61}$Co (2$\alpha$2p) | $2288 \pm 384$ | 2308 | $1721 \pm 251$ | 1817 | $1188 \pm 217$ | 1474 |

represented as

$$^{20}\mathrm{Ne}(^{16}\mathrm{O} + \alpha) + {}^{51}\mathrm{V} \Rightarrow {}^{67}\mathrm{Ga}^{*} + \alpha,$$
($\alpha$ as a spectator)
$$^{67}\mathrm{Ga}^{*} \Rightarrow {}^{61}\mathrm{Cu} + \alpha 2n.$$

3) *CF process:* in the case of the CF process, the incident projectile ($^{20}$Ne) fuses completely with the target nucleus ($^{51}$V) as a single entity. In this process, there is complete transfer of incident projectile's linear momentum to the resulting compound system. Thus, the third peak at highest recoil range in FRRDs of $^{61}$Cu residue (fig. 4) corresponds to the CF process. The excited intermediate compound system $^{71}$As$^{*}$ formed through the CF of $^{20}$Ne projectile with the $^{51}$V target will further decay via the 2$\alpha$2$n$, 2$\alpha$3$n$ and 2$\alpha$2p channels to form the ERs $^{61}$Cu, $^{60}$Cu and $^{61}$Co, respectively. The reaction mechanism for the formation of ER $^{61}$Cu through the CF process may be represented as

$$^{20}\mathrm{Ne} + {}^{51}\mathrm{V} \Rightarrow {}^{71}\mathrm{As}^{*},$$
$$^{71}\mathrm{As}^{*} \Rightarrow {}^{61}\mathrm{Cu} + 2\alpha 2n.$$

Extracting the relative contribution arising from CF, ICF$^{\alpha}$ and ICF$^{2\alpha}$ processes in the population of a given $\alpha$ emitting channel residue is still a challenging task as there is no theoretical model proposed so far for estimating the relative contribution arising from different fusion processes in the population of a given $\alpha$ emitting channel residue. Experimentally, the magnitude of relative contribution arising from CF, ICF$^{\alpha}$ and ICF$^{2\alpha}$ processes in the population of a given $\alpha$ channel residue can be estimated from the FRRDs of the populated ERs. The FRRDs of the $\alpha$ emitting channel residues comprise multiple peaks and the area under these peaks signifies the relative contribution arising from the corresponding fusion process.

Evaporation of nucleons from the recoiling compound system slightly modifies the recoil velocity and hence the recoil range of the ERs. The experimentally measured most probable range, $R_{exp}$, along with the theoretically estimated value using the code SRIM [31], $R_{theo}$, for all the identified ERs populated in the $^{20}$Ne+$^{51}$V reaction at $E_{lab} \approx 145$ MeV are tabulated in table 3. The full width at half maximum (FWHM) of the FRRDs increases with the increase in the number of evaporated particles from the excited compound system, reflecting the perturbing effect of these evaporated particles on the recoil velocity of the product combined with the effect of straggling and finite target thickness.

### 3.2 Universal Fusion Function (UFF): Estimating the incomplete fusion

In order to estimate the extent of fusion incompleteness in $^{20}$Ne induced reaction over $^{51}$V target, dimensionless physical quantities, fusion function $F(x)$ and $x$ have been formulated as

$$F(x) = \frac{2E_{c.m}}{R_b^2 \hbar w}\sigma_{CF}, \qquad x = \frac{E_{c.m} - V_b}{\hbar w}, \tag{3}$$

using the CF cross section, as prescribed by Canto *et al.* [20]. Here $R_b$, $V_b$ and $\hbar w$ denote the radius, height and curvature of the potential barrier, respectively. In order to compare the fusion cross section data of a given projectile over different targets, it is necessary to completely eliminate: a) the static effects of the interacting nuclei *viz.* size and Coulomb barrier and b) the dynamic effect of bound inelastic states and transfer coupling from the CF cross section. The formulation of the dimensionless variable $F(x)$ and $x$ completely eliminates the static as well as dynamic effects between the different fusing systems and makes them comparable. The reduction of CF cross section to fusion function $F(x)$ is derived from the Wong formula [21],

$$\sigma_{CF}(E_{c.m}) = \frac{R_b^2 \hbar w}{2E_{c.m}} \ln\left[1 + \exp\left(\frac{2\pi(E_{c.m} - V_B)}{\hbar w}\right)\right]. \tag{4}$$

Simplifying the Wong formula, $F(x)$ reduces to

$$F(x) = \ln[1 + \exp(2\pi x)] \tag{5}$$

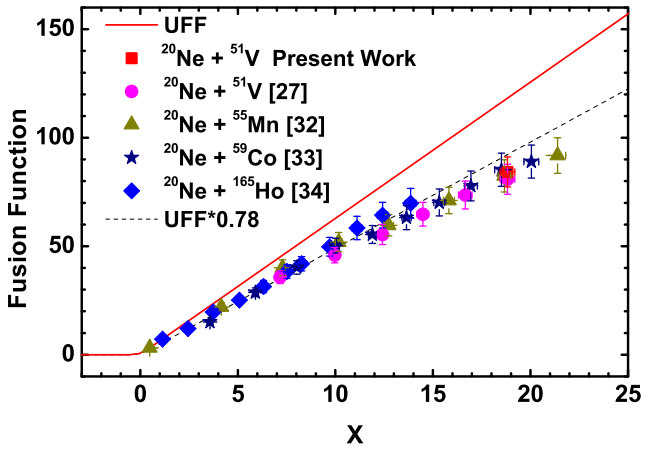


**Fig. 5.** (Color online) The CF fusion function $F(x)$ as a function of $x$ for the $\alpha$ cluster projectile $^{20}$Ne over different targets. The solid line represents the UFF and dotted line is the UFF multiplied by a suppression factor of 0.78.

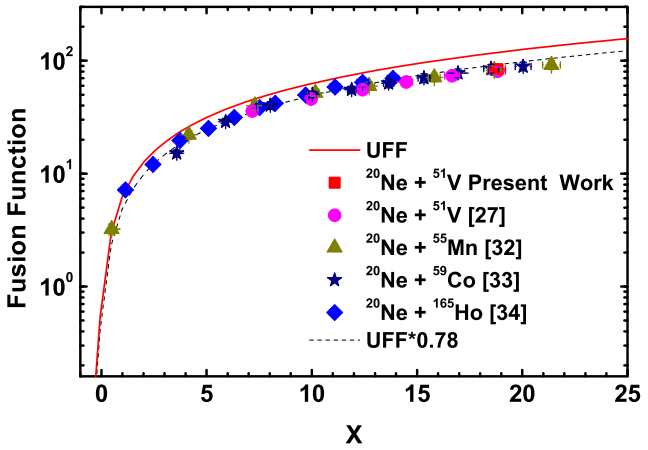


**Fig. 6.** (Color online) Same as fig. 5 except for the fact that the fusion function $F(x)$ is changed to logarithmic scale.

which is known as Universal Fusion Function (UFF). It can be noted that $F(x)$ is a simple function of the dimensionless variable $x$ and is independent of the interacting system. Thus, the CF cross section data of different systems can be compared directly with the help of UFF and systematics can be established. As inelastic excitation and transfer channel coupling are not so effective at energy above the Coulomb barrier, any deviation of experimental fusion cross section from UFF is attributed to the effect of projectile breakup on CF cross sections. The fusion function $F(x)$ for the $\alpha$ cluster projectile $^{20}$Ne over different targets, namely, $^{51}$V (present work) and ref. [27], $^{55}$Mn [32], $^{59}$Co [33] and $^{165}$Ho [34], as a function of $x$ is illustrated in fig. 5 and fig. 6. For the $^{20}$Ne projectile the most favorable breakup channel is $^{20}\text{Ne} \Rightarrow {}^{16}\text{O} + \alpha$ with an $E_{B.U}$ value of 4.7 MeV. In figs. 5 and 6, the solid line represents the UFF given by eq. (5). Suppression in CF fusion function with respect to UFF can be noted from figs. 5 and 6 for all the four systems. This suppression in $F(x)$ with respect to UFF is likely to be arising from the breakup of the $^{20}$Ne projectile into fragments owing to its low $E_{B.U}$ value.

### 3.3 Breakup fusion model: An analysis of ICF for the system $^{20}$Ne + $^{51}$V

According to the breakup fusion model for ICF reactions, proposed by Udagawa and Tamura [35], a breakup fragment (ejectile) is expected to move undeflected along the beam direction with a velocity approximately the same as that of the incident beam while the remaining part of the projectile fuses with the target nucleus with energy and momentum proportional to its relative mass with respect to the incident projectile.

Assuming that the ICF$^{\alpha}$ component in incompletely fused composite nuclei (IFC) $^{67}$Ga arises from breakup reaction of the type

$$^{20}\text{Ne}(^{16}\text{O} + {}^{4}\text{He}(\alpha)) + {}^{51}\text{V} \Rightarrow {}^{67}\text{Ga} + {}^{4}\text{He}(\alpha),$$

the excitation energy of the resulting IFC nucleus $^{67}$Ga can be calculated using the formula [36]

$$E^{*}_{^{67}\text{Ga}} = \left(\frac{4}{5}\right) E_{lab}(^{20}\text{Ne}) \left(\frac{51}{67}\right) + Q_{gg}, \qquad (6)$$

where $Q_{gg}$ is the ground state $Q$-value of the breakup reaction. The excitation energy of the IFC nucleus $^{67}$Ga was found to be 83.57 MeV at $E_{lab} = 145$ MeV. Applying the same criterion of the breakup fusion model on the ICF$^{2\alpha}$ process, formation of IFC nucleus $^{63}$Cu in the $^{20}\text{Ne} + {}^{51}\text{V}$ can be given by the reaction

$$^{20}\text{Ne}(^{12}\text{C} + {}^{8}\text{Be}(2\alpha)) + {}^{51}\text{V} \rightarrow {}^{63}\text{Cu} + {}^{8}\text{Be}(2\alpha).$$

The excitation energy of $^{63}$Cu calculated using the expression

$$E^{*}_{^{63}\text{Cu}} = \left(\frac{3}{5}\right) E_{lab}(^{20}\text{Ne}) \left(\frac{51}{63}\right) + Q_{gg} \qquad (7)$$

was found to be 58.52 MeV at $E_{lab} = 145$ MeV. Thus the excitation energy for the ICF$^{\alpha}$ as well as ICF$^{2\alpha}$ processes were found to be sufficiently above the threshold energy ($E_{thr}$) required for the formation of ERs, populated through these two processes.

Another important aspect of studying the ICF reaction is to look for whether it is occurring due to peripheral or central collision. The sum rule model, given by Wilczynski *et al.* [37], advocates the occurrence of ICF reactions through the peripheral collision. According to the sum rule model ICF reaction occurs for the angular momentum $\ell$ greater than or equal to the critical angular momentum ($\ell_{crt}$) for the CF reaction. For $\ell > \ell_{crt}$, the attractive pocket in the potential energy vanishes and, hence, fusion does not occur. Wilczynski [38] suggested that $\ell_{crt}$ for the colliding system can be calculated from the equilibrium condition of the Coulomb, nuclear and centrifugal forces as

$$2\pi(\gamma_1 + \gamma_2)\frac{C_1 C_2}{C_1 + C_2} = \frac{Z_1 Z_2 e^2}{(C_1 + C_2)^2} + \frac{\ell_{crt}(\ell_{crt}+1)\hbar^2}{\mu(C_1 + C_2)}, \qquad (8)$$

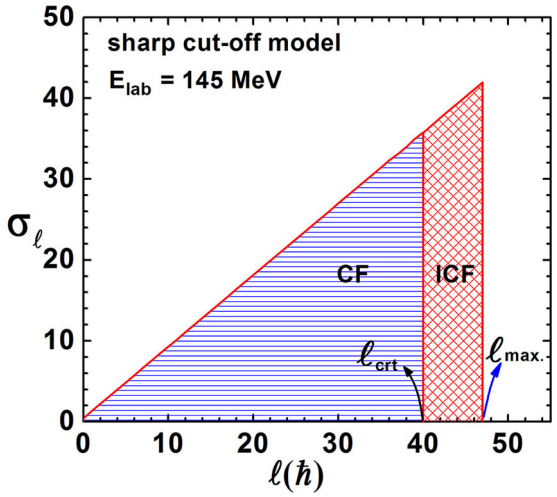


**Fig. 7.** (Color online) Sharp cut-off approximation for the $^{20}$Ne + $^{51}$V system at $E_{lab} = 145$ MeV. See text for details.

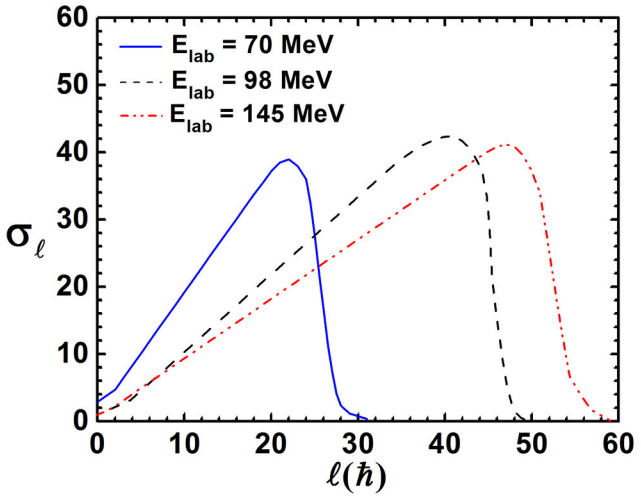


**Fig. 8.** (Color online) Predicted angular momentum distribution for the $^{20}$Ne + $^{51}$V system calculated using the code CCFULL at different energies ($E_{lab}$ = 70 MeV, 98 MeV and 145 MeV).

where $C_1$, $C_2$ are the half density radii and $\mu$ is the reduced mass of the binary system. The surface tension coefficients $\gamma_i$ were taken in this form

$$\gamma_i = 0.99\left\{1 - 1.78\left(\frac{N_i - Z_i}{A_i}\right)^2\right\}\ \text{MeV fm}^{-2}, \qquad (9)$$

which follows from the formula for the nuclear surface energy derived by Mayers [39]. When $\ell_{crt}$ is less than $\ell_{max}$, maximum possible angular momentum of a system at a given incident energy, the CF cross section may be calculated as

$$\sigma_{CF} = \frac{\pi\hbar^2}{2\mu E_{c.m}}\sum_{\ell=0}^{\ell_{crt}}(2\ell+1)T_\ell, \qquad (10)$$

where $T_\ell$ is the transmission coefficient for angular momentum $\ell$. According to sharp cut-off approximation [38], the transmission coefficient $T_\ell$ is given by

$$T_\ell = \begin{cases} 1, & \text{for } \ell \le \ell_{max}, \\ 0, & \text{for } \ell > \ell_{max}, \end{cases}$$

where $\ell_{max}$ corresponds to peripheral collision and is given by

$$\ell_{max} = R\sqrt{2\mu(E_{c.m} - V_B)/\hbar^2}. \qquad (11)$$

Here, $R$ is the maximum distance between two nuclei at which the collision leads to a nuclear reaction and $V_B$ is the fusion barrier of the system at a distance $R$. The concept of limiting angular momentum can be further explored by employing the sharp-cut off model to extract the value of $\ell_{crt}$ for the compound nuclei formed through the CF reaction. The nature of the sharp-cut off model assumption is shown in fig. 7 for the $^{20}$Ne + $^{51}$V system at $E_{lab} = 145$ MeV. The experimental fusion cross section ($\sigma_{CF}^{exp.}$) is needed to extract the $\ell_{crt}$. The stable residues observed in the present work have very little contribution to $\sigma_{CF}$. The remaining residues could not be detected due to their too short/long half-lives. The unaccounted cross section due to the formation of stable/unstable ERs in the present reaction were accounted for using the code PACE4 [40]. In the statistical model code PACE4, three important parameters were used in determining the various level densities needed for calculations. These are the "little-$a$" parameter involved in particle evaporation calculation, the ratio $a_f/a$ of the little-$a$ parameter at the saddle point and ground state deformations and $B_f$, the fission barrier, which is taken to be equal to the rotating liquid drop fission barrier. The little-$a$ parameter, which influences the equilibrium state components of the cross section is given as, $a = A/K$ where $A$ is the mass number of the compound nucleus and $K$ is an adjustable parameter, which may be varied to match the experimental data. In the present work the same value of $K$ is used ($K = 8$) which was used in ref. [27] for reproducing the experimental EF of the ERs populated through the CF channel in the $^{20}$Ne + $^{51}$V reaction in the energy range of 82–145 MeV. By using the code PACE4, the ratio $R = \Sigma\sigma_{pxn}^{PACE4}/\sigma_{fus}^{PACE4}$ ($x = 3, 4$) is calculated and using this ratio experimental CF cross section is calculated as $\sigma_{CF}^{exp.} = \Sigma\sigma_{pxn}^{exp.}/R$ [41]. The calculated values of $R$ and $\sigma_{CF}^{exp.}$ were found to be 0.002 and 679.21 mb, respectively, for the $^{20}$Ne + $^{51}$V system at $E_{lab} = 145$ MeV.

It is assumed that if all the reactions were of the complete fusion type, the angular momentum spectrum of the compound nuclei would be well approximated by a distribution function $f(\ell)$ such that

$$f(\ell)\mathrm{d}\ell = (2\ell/\ell_{max}^2)\mathrm{d}\ell, \quad \ell_{max} < \ell,$$
$$f(\ell)\mathrm{d}\ell = 0, \quad \ell_{max} > \ell,$$

where $\ell_{max}$ is given by eq. (11). The distribution of partial cross section ($\sigma_\ell$) as a function of $\ell$ has been obtained using the code CCFULL [42]. The results of CCFULL calculations are shown in fig. 8 for energies $E_{lab} = 70$, 98 and

**Table 4.** List of parameters used in PACE4 and CCFULL calculation for the system $^{20}\mathrm{Ne} + {}^{51}\mathrm{V}$ at $E_{lab} = 145\,\mathrm{MeV}$.

| | $V_b$ (MeV) | $R_b$ (fm) | $\hbar w$ (MeV) | $\ell_{max}$ ($\hbar$) |
|---|---|---|---|---|
| PACE4 | 32.33 | 6.6 | – | 52 |
| CCFULL | 33.4 | 8.7 | 4.06 | 47 |

145 MeV. As ICF reactions are expected to occur at the nuclear surface, the assumption is made that there exists a value of $\ell_{crt} < \ell_{max}$ such that the angular momentum distribution of the nuclei formed through the CF reaction is cut-off at $\ell_{crt}$. The value of $\ell_{crt}$ calculated using the prescription of Wilczynski *et al.* (eq. (8)) was found to be $38\hbar$ for the $^{20}\mathrm{Ne}+{}^{51}\mathrm{V}$ system. This value of $\ell_{crt}$ was found to be in good agreement with the $\ell_{crt}(= 39\hbar)$ value extracted from the experimental CF cross section data using the sharp cut-off approximations (eq. (10)). The value of $\ell_{max}(= 47\hbar)$ obtained from PACE4 as well as CCFULL calculation (table 4) was found to be sufficiently higher than $\ell_{crt}$ value, indicating that ICF reactions observed in the present work were arising mainly from the peripheral collision.

## 4 Conclusion

In order to investigate the role of partial LMT on incomplete fusion, measurement of FRRDs of the eight ERs, namely $^{67}$Ge(p3$n$), $^{66}$Ge(p4$n$), $^{65}$Ga($\alpha$2$n$), $^{63}$Zn($\alpha$p3$n$), $^{62}$Zn($\alpha$p4$n$), $^{61}$Cu(2$\alpha$2$n$), $^{60}$Cu(2$\alpha$3$n$) and $^{61}$Co(2$\alpha$2p), populated in the $^{20}\mathrm{Ne} + {}^{51}\mathrm{V}$ reaction at $E_{lab} \approx 145\,\mathrm{MeV}$, have been carried out. From the analysis of measured FRRDs of the populated ERs it is inferred that ERs populated through $\alpha$ emitting channels incorporates multiple component of LMT from the projectile to the target. The partial LMT from the projectile to the target is attributed to the fusion of $^{12}$C and $^{16}$O, arising from the breakup of the $^{20}$Ne projectile owing to its low $E_{B.U}$ value. A dimensionless fusion function $F(x)$ is deduced from the CF cross section data of the present work as well as for the $^{20}$Ne induced reactions over $^{51}$V, $^{55}$Mn, $^{59}$Co and $^{165}$Ho. On comparing the fusion function data with UFF, it is concluded that CF cross sections for the $^{20}$Ne induced reaction over different targets are suppressed. The CF suppression factor is determined by comparing the fusion function data with UFF calculation and is found to be about 22%. The $\ell_{crt}$ value, extracted from the experimental CF cross section as well as calculated using the prescription of Wilczynski [38] was found to be less than $\ell_{max}$, suggesting the peripheral nature of the observed ICF reactions.

One of the authors (SA) is thankful to UGC, New Delhi (INDIA) and MANUU, Hyderabad (INDIA) for providing financial assistance in the form of Minor Research Project grant (MANUU/Acad/F.404/2016-17/217) for carrying out this work. SA is also thankful to Dr. Md. Moin Shaikh, Research Associate, IUAC, New Delhi (INDIA) for fruitful discussions over the content of the manuscript and suggesting necessary inputs, and Principal, MANUU Polytechnic, Darbhanga (INDIA) for his conducive support and providing the basic facilities to carry out this work.

## References

1. H. Kumawat, V. Jha, V.V. Parkar, B.J. Roy, S.K. Pandit, R. Palit, P.K. Rath, C.S. Palshetkar, S.K. Sharma, S. Thakur, A.K. Mohanty, A. Chatterjee, S. Kailas, Phys. Rev. C **86**, 024607 (2012).
2. D.J. Hinde, M. Dasgupta, B.R. Fulton, C.R. Morton, R.J. Wooliscroft, A.C. Berriman, K. Hagino, Phys. Rev. Lett. **89**, 272701 (2002).
3. M.F. Guo, G.L. Zhang, P.R.S. Gomes, J. Lubian, E. Ferioli, Phys. Rev. C **94**, 044605 (2016).
4. Kamal Kumar, Tauseef Ahmad, Sabir Ali, I.A. Rizvi, Avinash Agarwal, R. Kumar, K.S. Golda, A.K. Chaubey, Phys. Rev. C **87**, 044608 (2013).
5. Avinash Agarwal, Sunil Dutt, Anjali Sharma, I.A. Rizvi, Kamal Kumar, Sabir Ali, Tauseeef Ahmad, Rakesh Kumar, A.K. Chaubey, EPJ Web of Conferences **38**, 17001 (2012).
6. F.K. Amanuel, B. Zelalem, A.K. Chaubey, Avinash Agarwal, I.A. Rizvi, Anjana Maheshwari, Tauseef Ahmed, Phys. Rev. C **84**, 024614 (2011).
7. H.E. Martz, R.G. Lanier, G.L. Struble, L.G. Mann, R.K. Sheline, W. Stoffl, Nucl. Phys. A **439**, 299 (1985) and references therein.
8. M. Afzal Ansari, R.K.Y. Singh, M.L. Sehgel, V.K. Mittal, D.K. Avasthi, I.M. Govil, Ann. Nucl. Energy **11**, 173 (1984) and references therein.
9. Abhishek Yadav, Vijay R. Sharma, Pushpendra P. Singh, Devendra P. Singh, R. Kumar, Unnati, M.K. Sharma, B.P. Singh, R. Prasad, R.K. Bhowmik, Phys. Rev. C **85**, 064617 (2012).
10. K. Surendra Babu, R. Tripathi, K. Sudarshan, S. Sodaye, A. Goswami, B.D. Shrivastava, B.S. Tomar, Nucl. Phys. A **739**, 229 (2004).
11. H.C. Britt, A.R. Quinton, Phys. Rev. **124**, 877 (1961).
12. F.K. Amanuel, B. Zelalem, A.K. Chaubey, Avinash Agarwal, I.A. Rizvi, Anjana Maheshwari, Tauseef Ahmed, Eur. Phys. J. A **47**, 156 (2011).
13. Abhishek Yadav, Vijay R. Sharma, Pushpendra P. Singh, Devendra P. Singh, Manoj K. Sharma, Unnati Gupta, R. Kumar, B.P. Singh, R. Prasad, R.K. Bhowmik, Phys. Rev. C **85**, 034614 (2012).
14. T. Inamura, M. Ishihara, T. Fakuda, T. Shimoda, H. Hiruta, Phys. Lett. B **68**, 51 (1977).
15. M. Dasgupta, D.J. Hinde, K. Hagino, S.B. Moraes, P.R.S. Gomes, R.M. Anjos, R.D. Butt, A.C. Berriman, N. Carlin, C.R. Morton, J.O. Newton, A. Szanto de Toledo, Phys. Rev. C **66**, 041602(R) (2002).
16. M. Dasgupta, D.J. Hinde, R.D. Butt, R.M. Anjos, A.C. Berriman, N. Carlin, P.R.S. Gomes, C.R. Morton, J.O. Newton, A. Szanto de Toledo, K. Hagino, Phys. Rev. Lett. **82**, 1395 (1999).
17. P.K. Rath, S. Santra, N.L. Singh, R. Tripathi, V.V. Parkar, B.K. Nayak, K. Mahata, R. Palit, Suresh Kumar, S. Mukherjee, S. Appannababu, R.K. Choudhury, Phys. Rev. C **86**, 051601(R) (2009).

18. M. Dasgupta, P.R.S. Gomes, D.J. Hinde, S.B. Moraes, R.M. Anjos, A.C. Berriman, R.D. Butt, N. Carlin, J. Lubian, C.R. Morton, J.O. Newton, A. Szanto de Toledo, Phys. Rev. C **70**, 024606 (2004) and references therein.
19. Md. Moin Shaikh, Subinit Roy, S. Rajbanshi, M.K. Pradhan, A. Mukherjee, P. Basu, S. Pal, V. Nanal, R.G. Pillay, A. Shrivastava, Phys. Rev. C **91**, 034615 (2015) and references therein.
20. L.F. Canto, P.R.S. Gomes, J. Lubian, L.C. Chamon, E. Crema, Nucl. Phys. A **821**, 51 (2009).
21. C.Y. Wong, Phys. Rev. Lett. **31**, 766 (1973).
22. Md. Moin Shaikh, Subinit Roy, S. Rajbanshi, M.K. Pradhan, A. Mukherjee, P. Basu, S. Pal, V. Nanal, R.G. Pillay, A. Shrivastava, Phys. Rev. C **90**, 024615 (2014).
23. M.F. Guo, G.L. Zhang, P.R.S. Gomes, J. Lubian, E. Ferioli, Phys. Rev. C **94**, 044605 (2016).
24. Abhishek Yadav, Vijay R. Sharma, Pushpendra P. Singh, R. Kumar, D.P. Singh, Unnati, M.K. Sharma, B.P. Singh, R. Prasad, Phys. Rev. C **86**, 014603 (2012).
25. Devendra P. Singh, Unnati, Pushpendra P. Singh, Abhishek Yadav, Manoj Kumar Sharma, B.P. Singh, K.S. Golda, Rakesh Kumar, A.K. Sinha, R. Prasad, Phys. Rev. C **80**, 14601 (2009).
26. Kamal Kumar, Tauseef Ahmad, Sabir Ali, I.A. Rizvi, Avinash Agarwal, R. Kumar, A.K. Chaubey, Phys. Rev. C **89**, 054614 (2014).
27. Sabir Ali, Tauseef Ahmad, Kamal Kumar, I.A. Rizvi, Avinash Agarwal, S.S. Ghugre, A.K. Sinha, A.K. Chaubey, J. Mod. Phys. **5**, 2063 (2014).
28. David Radford, Software package for interactive graphical analysis of gamma-ray coincidence data, `http://radware.phy.ornl.gov/`.
29. E. Browne, R.B. Firestone, *Table of Radioactive Isotopes* (Wiley, New York, 1986).
30. D.J. Parker, J.J. hogan, J. Asher, Phys. Rev. C **35**, 161 (1987).
31. J.F. Ziegler, *SRIM-2006, The Stopping Power and Range of Ions in Matter*, `http://www.srim.org/SRIM/SRIMLEGL.htm`.
32. Rahbar Ali, D. Singh, M. Afzal Ansari, M.H. Rashid, R. Guin, S.K. Das, J. Phys. G: Nucl. Part. Phys. **37**, 115101 (2010).
33. D. Singh, R. Ali, M. Afzal Ansari, B.S. Tomar, M.H. Rashid, R. Guin, S.K. Das, Phys. Rev. C **83**, 054604 (2011).
34. D. Singh, Rahbar Ali, M. Afzal Ansari, B.S. Tomar, M.H. Rashid, R. Guin, S.K. Das, Nucl. Phys. A **879**, 107 (2012).
35. T. Udagawa, T. Tamura, Phys. Rev. Lett. **45**, 1311 (1980).
36. S. Chakrabarty, B.S. Tomar, A. Goswami, G.K. Gubbi, S.B. Manohar, Anil Sharma, B. Bindukumar, S. Mukherjee, Nucl. Phys. A **678**, 355 (2000) and references therein.
37. J. Wilczynski, K. Siwek-Wilczynska, J. van Driel, S. Gonggrijp, D.C.J.M. Hageman, R.V.F. Janssens, J. Lukasiak, R.H. Siemssen, Phys. Rev. Lett. **45**, 606 (1980).
38. J. Wilczynski, Nucl. Phys. A **216**, 386 (1973).
39. W.D. Mayers, Nucl. Phys. A **204**, 465 (1973).
40. A. Gavron, Phys. Rev. C **21**, 230 (1980).
41. C.S. Palshetkar, S. Santra, A. Chatterjee, K. Ramachandran, Shital Thakur, S.K. Pandit, K. Mahata, A. Shrivastava, V.V. Parkar, V. Nanal, Phys. Rev. C **82**, 044608 (2010).
42. K. Hagino, N. Rowley, A.T. Kruppa, Comput. Phys. Commun. **123**, 143 (1999).